Research article

Journal of Applied Toxicology

Received: 2 August 2015, Accepted: 17 August 2015 Published online in Wiley Online Library: 5 October 2015

(wileyonlinelibrary.com) DOI 10.1002/jat.3233

Biodistribution and toxicity of spherical aluminum oxide nanoparticles

Eun-Jung Park[a*†], Gwang-Hee Lee[b†], Cheolho Yoon[c], Uiseok Jeong[d], Younghun Kim[d], Myung-Haing Cho[e] and Dong-Wan Kim[b*]

ABSTRACT: With the rapid development of the nano-industry, concerns about their potential adverse health effects have been raised. Thus, ranking accurately their toxicity and prioritizing for *in vivo* testing through *in vitro* toxicity test is needed. In this study, we used three types of synthesized aluminum oxide nanoparticles (AlONPs): γ-aluminum oxide hydroxide nanoparticles (γ-AlOHNPs), γ- and α-AlONPs. All three AlONPs were spherical, and the surface area was the greatest for γ-AlONPs, followed by the α-AlONPs and γ-AlOHNPs. In mice, γ-AlOHNPs accumulated the most 24 h after a single oral dose. Additionally, the decreased number of white blood cells (WBC), the increased ratio of neutrophils and the enhanced secretion of interleukin (IL)-8 were observed in the blood of mice dosed with γ-AlOHNPs (10 mg kg^{-1}). We also compared their toxicity using four different *in vitro* test methods using six cell lines, which were derived from their potential target organs, BEAS-2B (lung), Chang (liver), HACAT (skin), H9C2 (heart), T98G (brain) and HEK-293 (kidney). The results showed γ-AlOHNPs induced the greatest toxicity. Moreover, separation of particles was observed in a transmission electron microscope (TEM) image of cells treated with γ-AlOHNPs, but not γ-AlONPs or α-AlONPs. In conclusion, our results suggest that the accumulation and toxicity of AlONPs are stronger in γ-AlOHNPs compared with γ-AlONPs and α-AlONPs owing their low stability within biological system, and the presence of hydroxyl group may be an important factor in determining the distribution and toxicity of spherical AlONPs. Copyright © 2015 John Wiley & Sons, Ltd.

Additional Supporting Information may be found in the online version of this article:

Keywords: aluminum oxide nanoparticles; aluminum oxide hydroxide nanoparticles; toxicity; toxicity screening; distribution

Introduction

Aluminum is the third most abundant element in the Earth's crust, after oxygen and silica, and aluminum oxide has been widely used for many years in various fields, including the manufacturing, food, cosmetics and medicines (Krewski *et al*., 2007). Additionally, aluminum oxide hydroxide has applications in sol–gel ceramics, surface coatings and rheology control, it is also used in abrasives, cements, catalysts, and as a substrate for electronic circuits and refractory materials (Pailleux *et al*., 2013). With the rapid introduction of aluminum-based nanoparticles into the industry, their potential exposure has also dramatically increased, thus the Organization for Economic Co-operation and Development listed aluminum oxide nanoparticles (AlONPs) as high-priority groups in the program on the safety of manufactured nanomaterials in 2007. However, their safety is still under debate among toxicologists. For example, some researchers have suggested that AlONPs are less toxic than other metal-based nanomaterials (Lanone *et al*., 2009; Kim *et al*., 2010; Radzium *et al*., 2011; Sun *et al*., 2011; Demir *et al*., 2013). However, raw aluminum has been known to be a potential neurotoxin for a long time (Kumar and Gill, 2009). In addition, AlONPs have been demonstrated to induce cell death by impairing cellular components both *in vivo* and *in vitro* (Di Virgilio *et al*., 2010; Zhang *et al*., 2011; Alshatwi *et al*., 2012), as well as impairing innate cellular defenses against a respiratory pathogen (Braydich-Stolle *et al*., 2010).

The safety of nanomaterials should be confirmed prior to introduction into the market for the safe development of the nano-industry and nanotechnology. However, properties of nanomaterials can be altered in unpredictable ways according to both manufacturing and functionalizing methods, and animal testing is too costly and time-consuming. Thus, some researchers have suggested using *in vitro* toxicity screening to rank the toxicity of nanoparticles and prioritizing them for *in vivo* testing (Nel *et al*., 2006). Meanwhile, others raised some limitations in assessing the toxicity of nanoparticles using traditional *in vitro* toxicity test methods (Kroll *et al*., 2009; Monteiro-Riviere *et al*., 2009; Geys *et al*., 2010; Pailleux *et al*., 2013). For example, assay conditions, such as cell density, exposure concentration and exposure time, can influence the outcome of cytotoxicity testing. In addition,

*Correspondence to: Eun-Jung Park, Myunggok Eye Research Institute, Konyang University, 685, Gasuwon-dong, Seo-Gu, Daejeon, 302–718, Korea.
E-mail: pejtoxic@hanmail.net

Dong-Wan Kim, School of Civil, Environmental, Architectural Engineering, Korea University, Seoul, 136–713, Korea.
E-mail: dwkim1@korea.ac.kr

[a]Myunggok Eye Research Institute, Konyang University, Daejeon, 302-718, Korea

[b]School of Civil, Environmental, and Architectural Engineering, Korea University, Seoul, 136-713, Korea

[c]Seoul Center, Korea Basic Science Institute, Seoul, 126-16, Korea

[d]Department of Chemical Engineering, Kwangwoon University, Seoul, 139-701, Korea

[e]College of Veterinary Medicine, Seoul National University, Seoul, 151–742, Korea

[†]These authors contributed equally to this work.

Journal of Applied Toxicology

the toxic effects of metal-based nanoparticles are also dependent on their properties, including their types, their chemical composition and dispersion state, as well the properties of cells treated. Moreover, some researchers reported that the unique properties of nanoparticles can result in the misinterpretation of biological activity, leading to false-negative results in the classic toxicity assessment (Belyanskaya *et al*., 2007; Kroll *et al*., 2012). Herein, we synthesized three different types of AlONPs, α-AlONPs and γ-AlONPs, and aluminum oxide hydroxide nanoparticles (γ-AlOHNPs), and compared their distribution and biological responses *in vivo* (5 and 10 mg kg^{-1}). Then, we evaluated their toxicity in six cell lines, which were derived from the potential target organs of AlONPs (Park *et al*., 2010; Morsy *et al*., 2013; Park *et al*., 2015), using different four *in vitro* toxicity assessment tools.

Materials and methods

Preparation of AlONPs

Three types of AlONPs were prepared by a modification of a previously described method (Roh *et al*., 2011). The starting materials were $Al_2(SO_4)_3{\cdot}16H_2O$ (purity 95%; Fluka), Al(NO3)3·9H2O (purity 98%; Sigma-Aldrich, St. Louis, MO, USA) and urea (extra pure; Orient Chemical Industry, Osaka, Japan). The AlONPs were synthesized at a 0.215 concentration ratio of $Al_2(SO_4)_3{\cdot}16H_2O$ to $Al(NO_3)_3{\cdot}9H_2O$ using a forced hydrolysis method. In this technique, 0.0015 M $Al_2(SO_4)_3{\cdot}16H_2O$, 0.007 M $Al(NO_3)_3{\cdot}9H_2O$ and 0.1 M urea were mixed in 100 ml of deionize water (DW). The solution was placed in an oil bath at 90 °C to react for 1 h. The crude product was washed several times with DW to remove NO_3^- and SO_4^{2-}. The synthesized γ-AlOHNPs were then heat-treated in air at 900 °C and 1050 °C for 2 h to transform them into γ-AlONPs and α-AlONPs, respectively. Finally, three types of AlONPs (1 mg ml^{-1}) were dispersed in sterilized drinking water and DW for *in vivo* and *in vitro* test, respectively (Park *et al*., 2015).

Characterization of AlONPs

The morphology and crystalline phase of the AlONPs were characterized using transmission electron microscopy (TEM; FEI, Tecnai G2 F30 S-Twin) and X-ray diffraction (XRD; D/max-2500 V/PC, Rigaku). A simultaneous thermogravimetric method (TG; DTG-60 H, Shimadzu) was used for the thermal analysis of the γ-AlOOH nanospheres. The surface properties of the samples were investigated using a Fourier-transform infrared spectrometer (FT-IR; model 2000, Perkin-Elmer Inc., USA). The specific surface areas of the samples were estimated using a Brunauer–Emmett–Teller surface-area analyzer (BET; Belsorp mini II, BEL Japan Inc.), and the surface charge and hydrodynamic length in biocompatible fluids were characterized using a Zeta Potential and Particle Size Analyzer (ELSZ-2, Otsuka Electronics Korea Co. Ltd). Additionally, the surface charge and hydrodynamic length in vehicles were characterized using a Zeta Potential and Particle Size Analyzer (ELSZ-2, Otsuka Electronics Korea Co. Ltd.).

In vivo sample preparation

Six-week-old male ICR mice (27–28 g, OrientBio, Seongnam, Korea) were acclimatized for 1 week before the start of the study at a constant temperature of 23 ± 3 °C, with a relative humidity of 50 ± 10%, a 12-h light/dark cycle with a light intensity of 150–300 lux, and a ventilation of 10–20 times per h. After acclimation, three types of AlONPs (five mice per group) were single dosed orally (5 and 10 mg kg^{-1}), the control group was treated with sterilized drinking water, and mice were euthanized 24 h after a single dose. The experiments (IACUC No. 2012–0013) were assessed by the Institutional Animal Care and Committee (IACUC) of Ajou University (Suwon, Korea) and performed in accordance with the ILAR publication, 'Guide for the Care and Use of Laboratory Animals'.

Measurement of metal ion in tissues

Tissues were digested in a solution of HNO_3 (70%, 7 ml) and H_2O_2 (35%, 1 ml) using a microwave digestion system (Milestone, Sorisole, Italy) under high temperature and pressure (120 °C, 8 min; 50 °C, 2 min; 180 °C, 10 min). Concentrations of elements in the lysates were measured using an inductively coupled plasma mass spectrometry at the Korean Basic Science Institute (Supporting Information Table 1).

Hematological and cytokine analysis

Hematological analyzes of whole blood were conducted using a blood autoanalyzer (HemaVet850; CDC Technologies, Inc., Dayton, OH, USA). The whole blood was also centrifuged at 2000 g for 10 min to obtain serum for cytokine analysis. Concentrations of interleukin (IL)-6 (eBioscience, San Diego, CA, USA) and IL-8 (Cusabio, Wuhan, Hubei Province, China) were determined using commercially available enzyme-linked immunosorbent assay (ELISA) kits, according to the manufacturer's instructions (Park *et al*., 2015). Finally, the reactions were terminated by adding 1 M H_3PO_4; the absorbance was measured with an ELISA reader (Molecular Devices, Sunnyvale, CA, USA) at 450 nm. The amount of cytokine was calculated from a standard curve (0–1000 pg ml^{-1}), which was created under the same conditions.

Cell culture

Human bronchial epithelial cells (BEAS-2B) were purchased from ATCC (Manassas, VA, USA). Human embryonic kidney cells (HEK-293), rat cardiomyocytes (H9C2) and human brain glioblastoma cells (T98G) were purchased from the Korean Cell Line Bank (Seoul, Korea). Human keratinocytes (HACAT) and human liver cells (Chang) were kindly provided by Dr S.J. Kim (CHA University, Seoul, Korea). Cells were cultured in Dulbecco's modified Eagles's medium (DMEM)-F12 medium (BEAS-2B), RPMI medium (HEK-293) and DMEM medium (T98G, HACAT, Chang, and H9C2), in a humidified 5% CO_2 incubator at 37 °C. All mediums contained 10% heat-inactivated fetal bovine serum (GE Healthcare Life Sciences, Logan, Utah, USA), penicillin (100 units ml^{-1}) and streptomycin (100 μg ml^{-1}).

MTT assay

The 3-(4-5-dimethylthiazol-2-yl)-2,5-diphenyltetrazolium bromide (MTT, Sigma-Aldrich) assay was performed as previously described (Park *et al*., 2014b). Briefly, cells (1×10^4/well) were seeded into 96-well tissue culture plates and stabilized overnight. At 24 h after exposure with AlONPs (5 and 20 μg ml^{-1}), the MTT solution (2 mg ml^{-1}, 40 μl $well^{-1}$) was added, and the plate was incubated for 3 h at 37 °C. The cells were solubilized with dimethyl sulfoxide, and the absorbance was measured with a microplate spectrophotometer (Molecular Devices, Sunnyvale, CA, USA) at 540 nm. The viability of the treatment group was expressed as a percentage of the control group.

ATP measurement

Cells (1×10^4 cells per well) were seeded into 96-well white plates and stabilized overnight. At 24 h after exposure to AlONPs (5 and 20 μg ml^{-1}), a volume of CellTiter-Glo®Reagent (Promega, Madison, WI, USA) equal to the volume of culture medium was added to each well, and the contents were mixed for 2 min on an orbital shaker. The plate was incubated at room temperature (RT) for 10 min, and the luminescence value was measured using a microplate luminometer (Berthold detection systems, Berthold Technologies GmbH & Co. KG, Bad Wildbad, Germany) (Park *et al.*, 2014b).

LDH assay

The release of lactate dehydrogenase (LDH) was analyzed using commercially available LDH assay kits (Cat No. K313-500; Biovision, Milpitas, CA, USA) according to the manufacturer's instructions (Park *et al.*, 2014b). Briefly, cells (1×10^4 cells/well) were seeded in a 96-well plate and stabilized overnight. Cells were further incubated with or without AlONPs (5 and 20 μg ml^{-1}) for 24 h, and the supernatants (10 μl $well^{-1}$) were transferred to a new 96-well plate. The LDH reaction solution was added to each well, and the plate was incubated for 30 min at RT. The absorbance was measured with a microplate spectrophotometer (Molecular Devices) at 450 nm. A lysate solution in the kit was used for the positive control.

Real-time cell proliferation assay

Real-time cell proliferation was measured using an xCELLigence RTCA DP system (Roche Applied Science, Indianapolis, IN, USA). Briefly, cells (3×10^3 cells 100 μl^{-1} $well^{-1}$) were placed into an E-Plate 16 and stabilized overnight. Next, 100 μl of fresh medium with or without AlONPs (20 μg ml^{-1}) was added to each well, and then the cell proliferation was monitored for 48 h.

Statistical analysis

Data are the mean ± standard deviation (SD). All statistical analyzes were performed using Student's *t*-test (Prism 5; GraphPad Software, San Diego, CA, USA). Asterisks (*) indicate statistically significant differences from the control group (*$P < 0.05$ and **$P < 0.01$).

Results

Characterization of AlONPs

The morphology of the three types of AlONPs was characterized by TEM (Fig. 1A). A monodispersed, spherical morphology was observed for all the AlONPs (diameter 180–200 nm); the original spherical morphology of the γ-AlOHNPs was preserved even after treatment at high temperatures (Fig. 1A. a, c, and e). As expected, the selected area electron diffraction (SAED) pattern of γ-AlOHNPs revealed an amorphous nature (Fig. 1A. b). Fig. 1A (d) and (e) show that the other AlONPs had good crystallinity, corresponding to

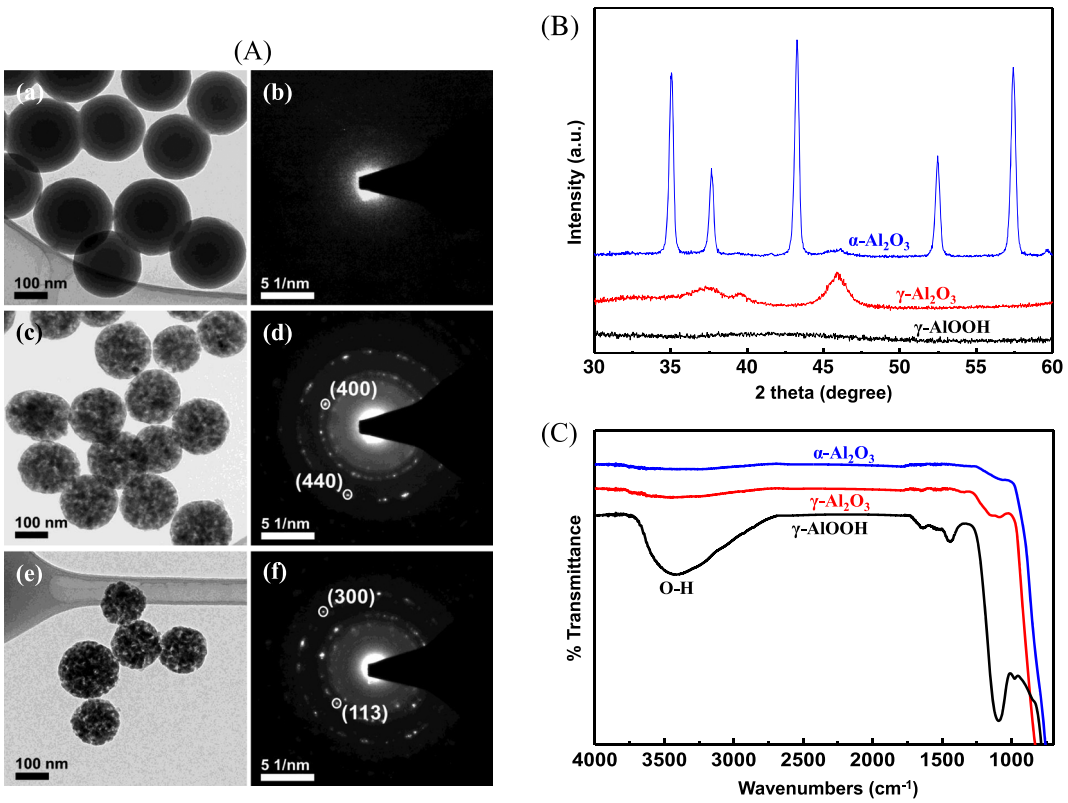

Figure 1. Physicochemical properties of three types of AlONPs. (A) Transmission electron microscope images (a, c, e) and corresponding selected area of electron diffraction patterns (b, d, f) of γ-aluminum oxide hydroxide nanoparticles (AlOHNPs), γ-AlONPs, and α-AlONPs, respectively. (B) X-ray diffraction patterns. As-prepared powders at 90°Cwere amorphous γ-AlOHNPs. After heat treatment at 900°C and 1050°C, crystalline γ-AlONPs and α-AlONPs were formed, respectively. (C) Fourier-transform infrared spectroscopy spectra of γ-AlOHNPs, γ-AlONPs, and α-AlONPs.

Journal of AppliedToxicology

Table 1. A summary of physicochemical characterization of aluminum oxide nanoparticles (AlONPs)

		Diameter (nm)	Surface charge (mV)
α-Al2O3	DW	476.6 ± 180.7	−43.8 ± 8.3
	Gastric fluid	540.7 ± 54.7	36.7 ± 1.2
	Intestinal fluid	712.6 ± 65.2	−17.02 ± 0.4
	Gamble's	1078.6 ± 75.3	−17.7 ± 0.1
	Cell culture media	193.7 ± 7.7	−13.6 ± 0.5
γ-AlOOH	DW	464.2 ± 293.6	−50.59 ± 8.67
	Gastric fluid	937.5 ± 111.3	26.3 ± 1.2
	Intestinal fluid	3178.8 ± 27.4	−18.1 ± 1.2
	Gamble's	1698.9 ± 232.0	−5.5 ± 0.0
	Cell culture media	2286.6 ± 326.0	−17.1 ± 1.2
γ-Al2O3	DW	786.3 ± 93.7	34.5 ± 2.3
	Gastric fluid	295.5 ± 29.3	23.2 ± 0.3
	Intestinal fluid	384.3 ± 79.1	−13.6 ± 1.8
	Gamble's	1663.1 ± 75.2	−11.3 ± 0.2
	Cell culture media	202.8 ± 7.1	−15.5 ± 0.4

γ-phases (PDF Card No. 02–1420) and α-phases (PDF Card No. 46–1212), respectively, which supports the XRD pattern observed in Fig. 1B. It is noteworthy that the porous structure of γ- and α-AlONPs was clearly observed by phase transformation during heat-treatment, compared with γ-AlOHNPs. This unique structure resulted in their relatively larger surface areas, as shown in the N_2 adsorption-desorption isotherms (Supporting Information Fig. 1). The presence of the hydroxyl functional groups in the γ-AlOHNPs was also confirmed using TG curve analysis (Supporting Information Fig. 2) and FT-IR spectroscopy (Fig. 1C). In addition, the hydrodynamic diameter of the γ-AlOHNPs became greater in artificial body fluids compared with the others (Table 1). Furthermore, surface charges on both α-AlONPs and γ-AlOHNPs were negative in DW, but that on γ-AlONPs was positive.

Comparison of bioaccumulation in mice

To compare accumulation level in mice of three types of AlONPs (5 mice/group), we euthanized mice 24 h after a single dose (Fig. 2, 5 and 10 mg/kg). Table 2 shows the tissue accumulation of AlONPs 24 h after a single dose. As compared with the control, the accumulation level in tissues was the highest in the mice administered with γ-AlOHNPs, followed by γ-AlONPs. In addition, the three AlONPs accumulated most in the liver, followed by the lung and kidney.

Comparison of biological effect following bioaccumulation of AlONPs

The presence of excess nanoparticles can trigger the subsequent adverse health effects by generating reactive-oxygen species (ROS) in biological systems. Herein, we first measured the changes in tissue homeostasis of the redox response-related elements after the accumulation of AlONPs. As results, the levels of manganese (Supporting Information Table 2A), copper (Supporting Information Table 2B), zinc (Supporting Information Table 2C) and iron (Supporting Information Table 2D) were altered in the tissues of mice dosed with AlONPs, especially γ-AlOHNPs. The number of white blood cells (WBC) significantly decreased in mice dosed with γ-AlOHNPs (10 mg kg^{-1}, Table 3) compared with the control, whereas that clearly increased in mice dosed with γ-AlONPs (10 mg kg^{-1}). In addition, as compared with the control, the portion of neutrophils in WBC increased in mice dosed with γ-AlOHNPs (10 mg kg^{-1}), whereas the number of platelets was significantly reduced in mice dosed with γ-AlOHNPs. Then, we measured the levels of pro-inflammatory mediators, IL-6 and IL-8, in the blood.

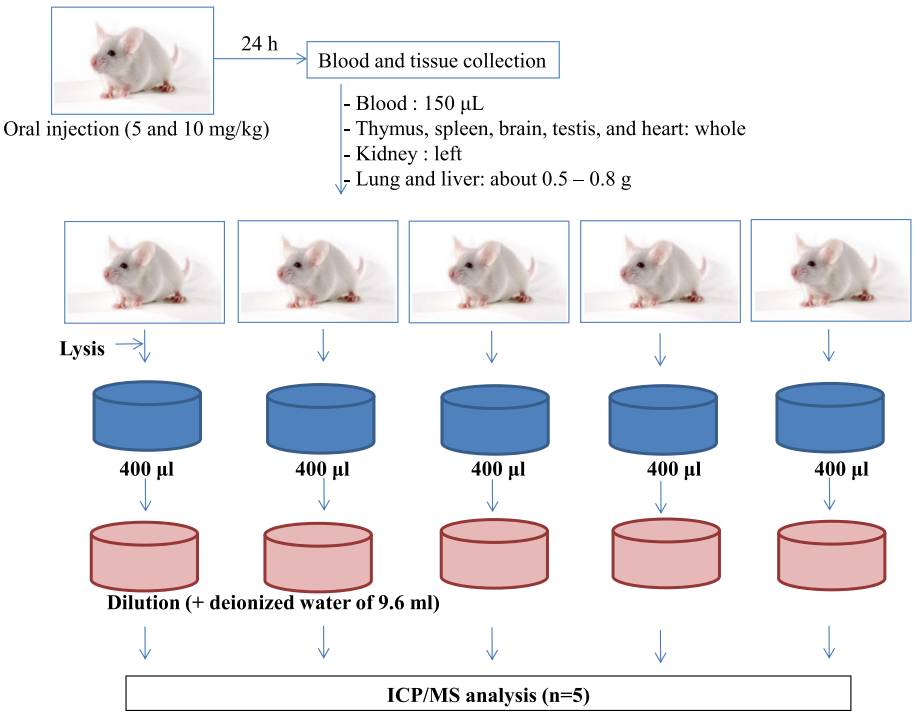

Figure 2. *In vivo* experimental design.

Table 2. Aluminum level in tissues

Aluminum	Brain (ng/g)	Thymus (ng/g)	Heart (ng/g)	Lung (ng/g)	Liver (ng/g)	Kidney (ng/g)	Spleen (ng/g)	Testis (ng/g)	Blood (ng/μL)
Control	1243.3±181.5	5587.1±899.5	2402.1±387.3	1876.9±193.4	497.1±121.7	924.6±277.3	3633.3±648.5	1921.7±465.0	1.5±0.2
α-AlONPs (5)	1208.9±56.0	5367.4±224.1	4498.6±1484.1	2647.7±0.6**	830.6±173.3**	1258.3±179.5*	3419.8±268.0	2866.0±684.3	2.8±0.2**
α-AlONPs (10)	923.0±238.7*	5397.4±2737.3	2561.4±701.6	2415.7±846.5	602.1±123.4	1031.0±449.3	2791.8±955.8	1992.5±370.6	2.8±0.7**
γ-AlOHNPs (5)	1160.2±167.2	7799.3±2694.9	3581.3±552.9**	3199.0±695.5**	803.2±136.6**	1185.8±220.0	6188.0±892.1**	2998.9±435.8	3.4±0.8**
γ-AlOHNPs (10)	1545.1±299.1*	7334.4±700.1	3886.5±559.3**	3619.1±380.1**	1010.6±295.2**	1887.6±559.7**	6776.4±987.0**	3752.0±517.1**	3.7±0.2**
γ-AlONPs (5)	1433.6±418.7	6033.1±1470.6	2960.8±454.0*	2548.8±444.2*	809.2±191.4**	1178.0±39.6	4311.9±357.2	2778.4±81.4**	2.9±0.5**
γ-AlONPs (10)	1154.0±180.4	6092.1±588.5	3597.5±449.8**	2370.9±73.8**	844.1±175.8**	1285.6±324.6	4913.6±2508.8	3635.3±613.8**	2.5±0.2**

Each tissue was harvested from mice (5 mice per group) 24 h after a single oral dose. Results represent the mean ± SD ($n = 5$).
* $P < 0.05$
** $P < 0.01$

Table 3. Hematological changes in mice dosed with aluminum oxide nanoparticles (AlONPs)

Name	WBC	LY	MO	NE	EO	BA	RBC	MCV	HCT	MCH	MCHC	Hgb	RDW	PLT	MPV
Control	3.9±0.3	89.7±1.5	3.0±0.1	6.2±0.4	0.8±1.0	0.4±0.3	7.2±0.8	59.4±4.2	43.1±8.0	17.1±0.2	28.9±1.7	12.4±1.6	16.5±0.7	1380.0±265.9	6.2±0.5
α-AlONPs (5)	3.9±1.3	82.2±13.7	4.8±3.8	11.8±9.6	0.6±0.3	0.6±0.5	6.8±0.7	57.3±5.0	39.0±6.4	16.2±1.3	28.2±0.2	11.0±1.8	16.9±0.9	1250.7±165.7	6.6±0.6
α-AlONPs (10)	5.2±1.5	87.5±4.6	3.4±1.2	3.4±1.2	0.7±0.2	0.5±0.2	7.2±0.4	61.7±1.7	44.3±2.3	16.8±1.1	27.2±1.0	12.1±0.8	16.0±0.5	1426.0±110.0	6.1±0.2
γ-AlOHNPs (5)	3.1±1.2	87.3±3.9	3.3±1.0	8.3±2.4	0.4±0.3	0.8±0.5	7.6±0.7	59.8±4.3	45.6±5.2	17.3±1.1	28.9±0.8	13.1±1.2	16.7±0.7	948.5±382.5*	6.9±1.0
γ-AlOHNPs (10)	2.5±0.6**	86.3±0.6	3.1±0.6	9.8±0.2**	0.3±0.2	0.6±0.1	7.2±0.7	56.9±0.2	41.1±4.1	16.9±0.4	29.7±0.8	12.2±1.0	16.9±0.2	1024.3±234.5*	6.9±0.2*
γ-AlONPs (5)	2.9±0.8	88.8±2.5	3.2±1.0	7.0±1.5	0.5±0.0	0.5±0.1	7.0±0.6	60.2±2.9	41.9±2.8	17.0±0.2	28.2±1.0	11.8±1.0	16.2±0.7	1405.0±194.1	6.3±0.3
γ-AlONPs (10)	5.0±0.6**	90.1±2.6	3.1±0.8	6.3±1.6	0.2±0.2	0.4±0.2	7.7±0.7	61.4±0.9	46.9±4.2	17.1±0.6	28.0±0.9	13.2±1.3	16.2±0.2	1282.0±372.2	6.4±1.1

Blood was collected from mice (five mice per group, $n = 5$) 24 h after a single dose. Results represent the mean ± SD.
* $P < 0.05$
** $P < 0.01$

Journal of AppliedToxicology

As compared with the control, the level of IL-8 was significantly enhanced in AlONPs-treated mice (Fig. 3), whereas the level of IL-6 was not changed in any of the treated groups (data not shown).

Comparison of the effect on cell viability

A dose-dependent decrease in cell viability was observed in all tested cell lines (Fig. 4), and the degree of toxicity was generally in order of α-AlONPs, γ-AlONPs and γ-AlOHNPs. While the toxic effects of α- and γ-AlONPs were strongest in the HACAT cells, followed by the BEAS-2B cells, that of γ-AlOHNPs was strongest in the BEAS-2B cells, followed by the H9C2 and HEK-293 cells.

Comparison of effects on ATP production

γ-AlOHNPs remarkably decreased ATP production compared with the control (Fig. 5), and the decreased level was highest in the BEAS-2B cells, followed by HEK-293, H9C2 and Chang cells. α-AlONPs also significantly reduced ATP production in H9C2 and HEK-293 cells. However, γ-AlONPs did not induce significant changes in ATP production in any of the six cell lines used in this study.

Comparison of effects on LDH release

As compared with the control, γ-AlOHNPs dose-dependently elevated the LDH level in all the cell lines tested, and the elevated

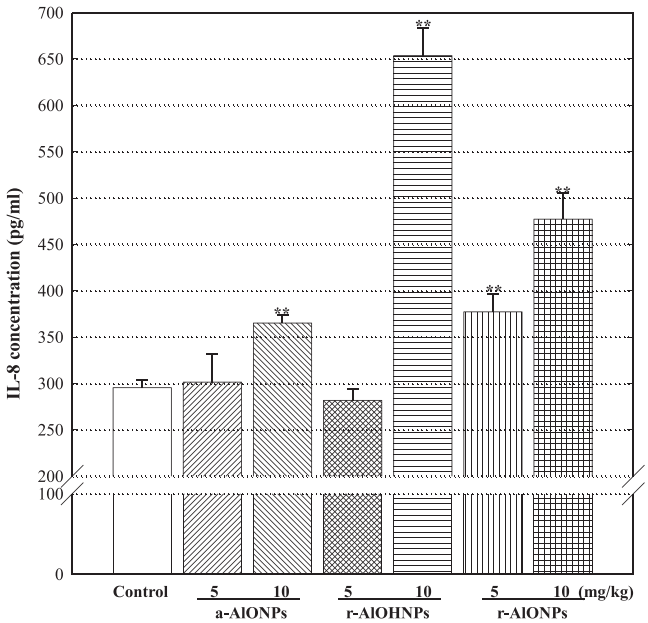

Figure 3. IL-8 levels in blood. Blood was collected from mice (5 mice/group) 24 h after a single oral dose. The standard curve was constructed under the same condition (0–1,000 pg ml^{-1}), and the values were presented as mean ± SD. *$P < 0.05$; **$P < 0.01$.

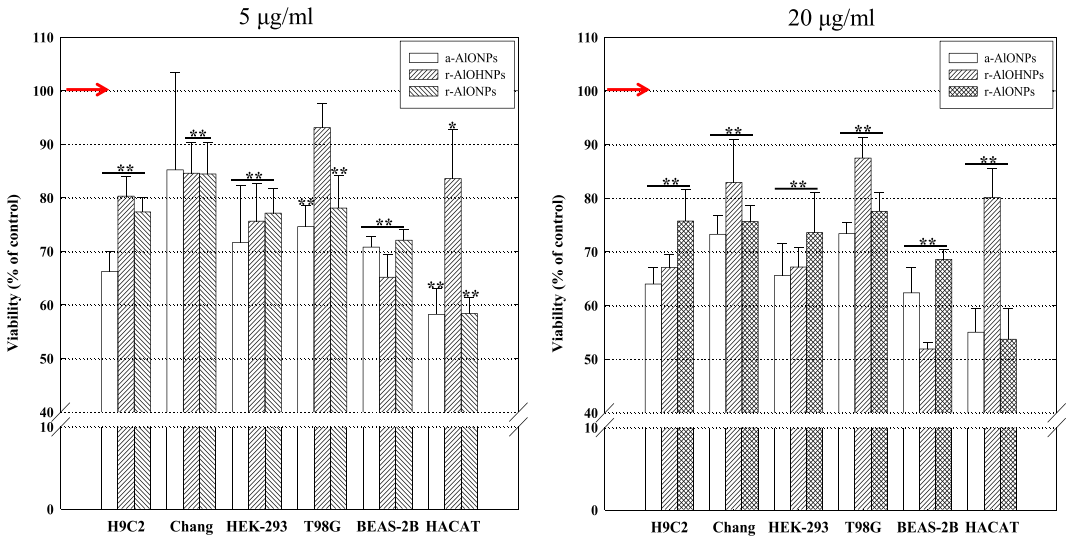

Figure 4. Comparison of cytotoxicity based on the MTT assay. Cells were treated with AlONPs (5 or 20 μg mL^{-1}) for 24 h. Each experiment was measured using five wells per concentration. The results are mean ± SD of three independent experiments. Viability of the treatment group was expressed as a percentage of the control group (100 %). *$P < 0.05$; **$P < 0.01$.

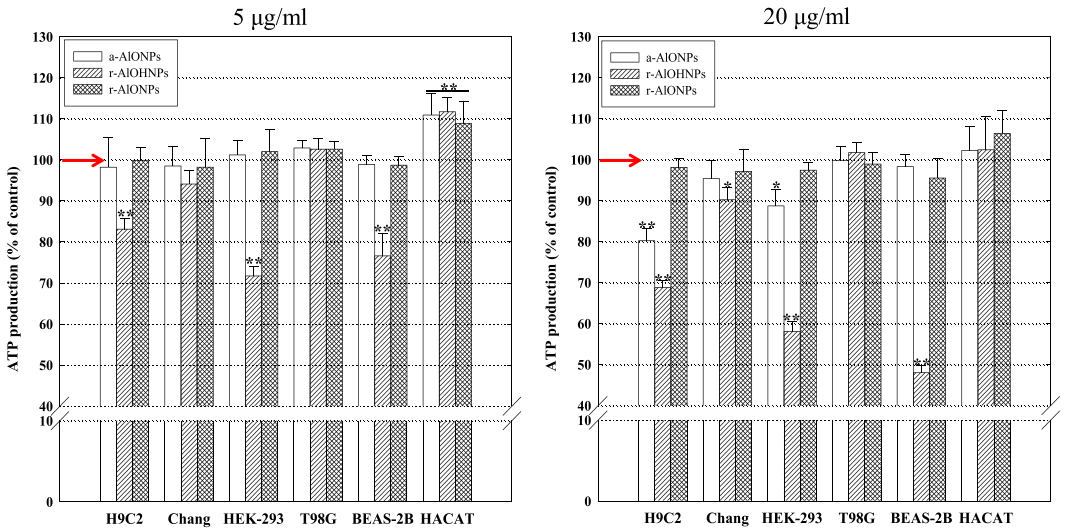

Figure 5. Comparison of effects on ATP production. Cells were treated with AlONPs (5 or 20 μg mL^{-1}) for 24 h. Each experiment was performed using five wells per concentration, and the experiment was performed independently three times. Results (mean ± SD) were expressed as a percentage of the control group *$P < 0.05$; **$P < 0.01$.

level was the highest in the HEK-293 cells, followed by BEAS-2B cells (Fig. 6). Additionally, the LDH level was significantly increased in H9C2 and HACAT cells treated with α-AlONPs, but γ-AlONPs did not induce a significant change in any of the cell lines tested.

Comparison of the effect of cell proliferation

As shown in Fig. 7, cells exposed to γ-AlOHNPs proliferated slowly compared with cells exposed to α- and γ-AlONPs. In addition, both BEAS-2B and H9C2 cells exposed to γ-AlOHNPs did not proliferate until 48 h after exposure, thus the number of cells decreased with time.

Discussion

With the dramatic increase in the development of nanotechnology, the public's concern about the potential adverse effects of nanoparticles on human health and the environment has also rapidly increased. Therefore, the global effort to produce and collect toxicological data on nanomaterials has accelerated to prevent the onset of unexpected adverse effects after exposure. However, the physicochemical properties of nanomaterials are enormously variable depending on the manufacturing process, it is also predicted that their toxicity may different according to their unique properties. Thus, researchers have been trying to prioritize animal experiments by screening in cell-based systems and to determine the correlation between the results obtained from *in vitro* and *in vivo* toxicity assessments (Nel *et al.*, 2006, 2013).

The physicochemical properties of manufactured nanoparticles are important factors for interactions between nanoparticles and biology (Nel *et al.*, 2009). Similarly, the properties of manufactured nanoparticles can be changed easily in biocompatible vehicles used for the toxicity test, such as deionized water, drinking water, phosphate-buffered saline and cell culture media, and within the

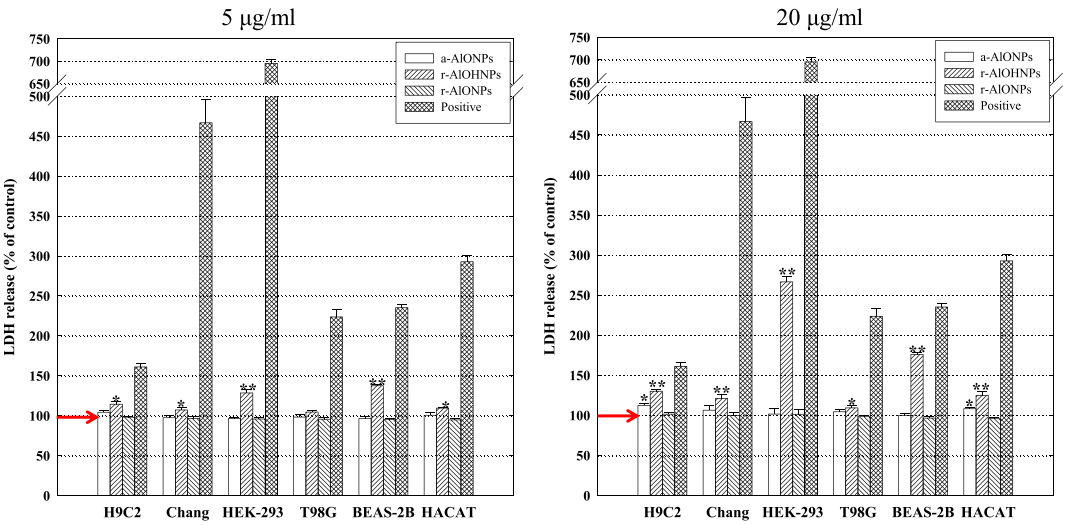

Figure 6. Comparison of effects on LDH release. Cells were treated with AlONPs (5 or 20 μg mL^{-1}) for 24 h. Five wells per concentration were measured, and the experiment was performed independently three times. Results (mean ± SD) were expressed as a percentage of the control group. *$P < 0.05$; **$P < 0.01$.

Journal of AppliedToxicology

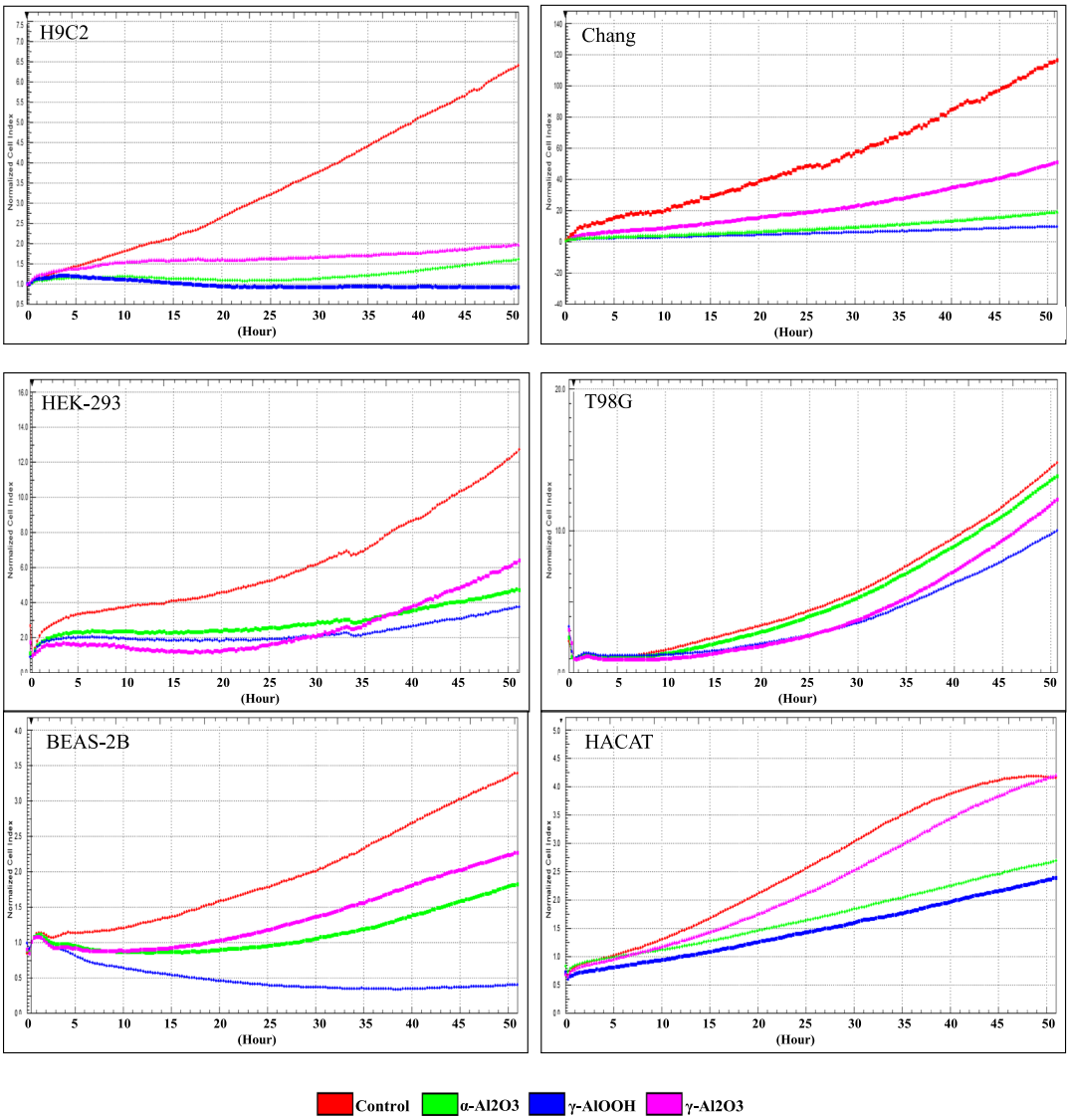

Figure 7. Comparison of effects on real-time cell proliferation. Cells were treated with AlONPs (5 or 20 μg/mL), and monitored for at least 48 h after exposure. Graphs were plotted using the mean value of 4 wells (4 wells/sample).

biological system, uptake level, uptake speed and resultant toxic effects of nanoparticles can be also influenced by these altered properties (Wagner *et al*., 2007; Walkey and Chan, 2012; Panariti *et al*., 2012; Cheng, 2013; Duan and Li, 2013; Kettiger *et al*., 2013; Luengo *et al*., 2013; Braakhuis *et al*., 2014). Therefore, we should concurrently consider these properties for accurate interpretation of toxicity data. First, aluminum oxide is an amphoteric substance, which can react with both acids and bases and has excellent hardness and a high melting point. Its most common form is the α-Al_2O_3 phase, but it also exists in other forms that have unique crystal structures and properties. Additionally, γ-AlOHNPs, as prepared in this present study, are prone to decomposition. The weight loss (roughly 57.8%) at 1200 °C corresponds to the removal of physisorbed (physically adsorbed) water as well as the further release of water accompanying phase transformation (γ-AlOOH → γ-Al_2O_3 → α-Al_2O_3) (Roh *et al*., 2011; Yue *et al*., 2011). Therefore, it can be understood that the porous nature of γ- and α-AlONPs originated from the thermal decomposition of γ-AlOHNPs. Furthermore, a broad band appearing at 3417 cm^{-1} on the FT-IR reveals the presence of hydroxyl groups (OH^-) (El-Naggar, 2013), additional peaks appearing in the region from 1090 to 1650 cm^{-1} are representative of physisorbed water. This hydration effect could result in the distinct weight loss during heat treatment, as shown in the TG analysis (Supporting Information Fig. 2) (Karim *et al*., 2011). However, the OH^--bonding character was significantly disappeared in γ- and α-AlONPS by the thermal decomposition at high temperatures. Furthermore, nanoparticles tended to accumulate easily and to be more harmful to the body than micro-sized particles, because of their small size and wide surface area. It has also been shown that positively charged nanoparticles pass through the cell membrane more easily than the negatively charged particles because of electrostatic effects. In this study, the three types of AlONPs were observed to aggregate highly in DW and drinking water. However, in cell culture media, while the aggregation of α- and γ-AlONPs reduced, that of γ-AlOHNPs was enhanced. In addition, the surface charge on γ-AlONPs was positive, unlike the charge on the other two AlONPs. Therefore, we can predict that uptake through the cell membrane would probably occur in order of γ-AlONPs, α-AlONPs, and γ-AlOHNPs, and that the accumulated level of γ-AlOHNPs in mice may be lower compared

with those of α- and γ-AlONPs. However, contrary to expectations, γ-AlOHNPs accumulated the most 24 h after administration. Similarly, the secretion of a pro-inflammatory chemokine and the disturbance in the homeostasis of the redox response-related elements were the highest when dosed with γ-AlOHNPs (Supporting Information Table 2 and Fig. 3). According to a previous report, when the particles were inhaled, there was no significant difference between the lung burden levels of particles 0.5 μm in size or 3 μm in size (Oberdorster *et al*., 2005). In addition, separation of particles was observed in a TEM image of cells treated with γ-AlOHNPs, but not γ-AlONPs or α-AlONPs (Supporting Information Fig. 4). Therefore, we hypothesize that the high accumulation of γ-AlOHNPs may be attributed to a weaker strength (structural stability), and the biological effects of AlONPs could be strengthened in the presence of a hydroxyl group.

In vitro tests have traditionally been used to screen the toxicity of chemicals because they are simple and time- and cost-efficient when compared with *in vivo* assays (Kroll *et al*., 2009). However, *in vitro* assays lack the complexity, metabolic activity and the kinetics of animal models because they are not systemic. Considering that the properties of a biological system are important factors determining the toxicity of nanoparticles as well those of nanoparticles, the selection of cell lines is very important in order to increase the validity of data from *in vitro* tests. In the present study, we used six cell lines derived from the potential target organs of the nanoparticles: BEAS-2B (lung), Chang (liver), HACAT (skin), H9C2 (heart), T98G (brain) and HEK-293 (kidney). The lungs and skin are major exposure routes for nanoparticles, and the liver, heart, kidney and brain have been found to be major target organs after oral administration (Park *et al*., 2010, 2014; Morsy *et al*., 2013). Furthermore, current cytoxicity testing for nanoparticles is based on *in vitro* methods established for hazard characterization of chemicals, such as the MTT assay, LDH release assay, annexin V and propidium iodide staining, and neutral red staining. However, evidence is accumulating that nanoparticles differ greatly from existing chemicals and may interfere with commonly used test systems. For example, nanoparticles led to false-negative results by interacting with the substrate in MTT assays (Belyanskaya *et al*., 2007; Kroll *et al*., 2009). Similarly, some nanoparticles present in the reaction mixture, inside cells, or absorbed on cells may directly influence the measurements by increasing the light absorption owing to their optical properties (Barillet *et al*., 2010). In addition, metal-based nanoparticles may attenuate indications of necrosis by inhibiting the LDH release (Kroll *et al*., 2009, 2012). Cytokines, a group of inflammatory extracellular mediators, can also be adsorbed onto the surface of nanoparticles, resulting in an underestimation of the quantity released (Pailleux *et al*., 2013). As well, nanoparticles can lead to underestimation of the number of ROS-generating cells by quenching the fluorescence of dichlorofluorescin diacetate, a substrate used to measure ROS (Aam and Fonnum, 2007; Kroll *et al*., 2012). Considering these findings, we compared the toxicities of three types of AlONPs using four viability assays with different detection principles. First, based on the MTT assay, three types of AlONPs significantly decreased viability in all the cell lines tested, and γ-AlOHNPs induced lower toxicity than the others in HACAT, T98G and Chang cells. However, the ATP level was not significantly altered in T98G and HACAT cells exposed to three types of AlONPs, and γ-AlONPs were non-toxic for all the six cell lines tested. Additionally, based on the results of the LDH assay, which evaluates membrane damage, γ-AlOHNPs induced greater damage than the α- and γ-AlONPs in the six cell lines tested, especially in HEK-293 and BEAS-2B cells. Moreover, in the real-time proliferation assay, which measures electrical impedance on the plate bottom, α- and γ-AlONPs generally restored proliferation speed with time, but BEAS-2B and H9C2 cells exposed to γ-AlOHNPs (20 μg ml^{-1}) did not proliferate until 48 h after exposure. Therefore, we suggest that BEAS-2B cells exposed to γ-AlOHNPs may induce the highest toxicity, although results from toxicity assessment tools used in this study conflicted (Park *et al*., 2014). Furthermore, the MTT assay and ATP assay are used to assess effects on mitochondrial function, whereas the LDH assay evaluates membrane integrity. Also, the MTT and LDH assay detect the amount of the light transmitted through the well plate, and the ATP assay measures the light emitted by the samples during the reaction. While the MTT assay measures formazan directly from the live cells on the well plate, the LDH assay uses only a part (10 μl) of the supernatant. Therefore, results from the MTT assay may be influenced by the uptake of nanomaterials into the cells compared with those from the LDH assay.

In conclusion, our study clearly highlights that the presence of hydroxyl groups are an important factor in determining the toxicity of spherical AlONPs. In addition, the choice of cell types and cytotoxicity assessment tools should be carefully considered during the toxicity screening of nanoparticles.

Acknowledgments

This work was supported by the Basic Science Research Program, through the National Research Foundation of Korea, funded by the Ministry of Education, Science and Technology (2011-35B-E00011, 2012R1A2A2A01045382).

Conflict of interest

The authors report no conflicts of interest to declare.

References

Aam BB, Fonnum F. 2007. Carbon black particles increase reactive oxygen species formation in rat alveolar macrophages in vitro. *Arch. Toxicol.* **81**: 441–446.

Alshatwi AA, Vaiyapuri Subbarayan P, Ramesh E, Al-Hazzani AA, Alsaif MA, Alwarthan AA. 2012. Al2O3 nanoparticles induce mitochondria-mediated cell death and upregulate the expression of signaling genes in human mesenchymal stem cells. *J. Biochem. Mol. Toxicol.* **26**: 469–476.

Barillet S, Simon-Deckers A, Herlin-Boime N, Mayne-L'Hermite M, Reynaud C, Cassio D, Gouge B, Carrière M. 2010. Toxicological consequences of TiO2, SiC nanoparticles and multi-walled carbon nanotubes exposure in several mammalian cell types: an in vitro study. *J. Nanopart. Res.* **12**: 61–73.

Belyanskaya L, Manser P, Spohn P, Bruinink A, Wick P. 2007. The reliability and limits of the MTT reduction assay for carbon nanotubes-cell interaction. *Carbon* **45**: 2643–2648.

Braydich-Stolle LK, Speshock JL, Castle A, Smith M, Murdock RC, Hussain SM. 2010. Nanosized aluminum altered immune function. *ACS Nano* **4**: 3661–3670.

Braakhuis HM, Park MV, Gosens I, De Jong WH, Cassee FR. 2014. Physicochemical characteristics of nanomaterials that affect pulmonary inflammation. *Part. Fibre Toxicol.* **11**: 18.

Cheng LC, Jiang X, Wang J, Chen C, Liu RS. 2013. Nano-bio effects: interaction of nanomaterials with cells. *Nanoscale* **5**: 3547–3569.

Demir E, Burgucu D, Turna F, Aksakal S, Kaya B. 2013. Determination of TiO2, ZrO2, and Al2O3 nanoparticles on genotoxic responses in human peripheral blood lymphocytes and cultured embryonic kidney cells. *J. Toxicol. Environ. Health A* **76**: 990–1002.

Di Virgilio AL, Reigosa M, de Mele MF. 2010. Response of UMR 106 cells exposed to titanium oxide and aluminum oxide nanoparticles. *J. Biomed. Mater. Res. A* **92**: 80–86.

Duan X, Li Y. 2013. Physicochemical characteristics of nanoparticles affect circulation, biodistribution, cellular internalization, and trafficking. *Small* **9**: 1521–1532.

El-Naggar AY. 2013. Characterization of modified and polymer coated alumina surfaces by infrared spectroscopy. *J. Spectrosc.* **706960**: 5.

Geys J, Nemery B, Hoet PH. 2010. Assay conditions can influence the outcome of cytotoxicity tests of nanomaterials: better assay characterization is needed to compare studies. *Toxicol. In Vitro* **24**: 620–629.

Karim MR, Rahman MA, J. Miah MA, Ahmad H, Yanagisawa M, Ito M. 2011. Synthesis of γ-alumina particles and surface characterization. *The Open Colloid Sci. J.* **4**: 32–36.

Kettiger H, Schipanski A, Wick P, Huwyler J. 2013. Engineered nanomaterials uptake and tissue distribution: from cell to organism. *Int, J, Nanomed.* **8**: 3255–3269.

Kim IS, Baek M, Choi SJ. 2010. Comparative cytotoxicity of Al2O3, CeO2, TiO2 and ZnO nanoparticles to human lung cells. *J. Nanosci. Nanotechnol.* **10**: 3453–3458.

Krewski D, Yokel RA, Nieboer E, Borchelt D, Cohen J, Harry J, Kacew S, Lindsay J, Mahfouz AM, Rondeau V. 2007. Human health risk assessment for aluminium, aluminium oxide, and aluminium hydroxide. *J. Toxicol. Environ. Health B Crit. Rev.* **10**(Suppl 1): 1–269.

Kroll A, Pillukat MH, Hahn D, Schnekenburger J. 2009. Current in vitro methods in nanoparticle risk assessment: limitations and challenges. *Eur. J. Pharm. Biopharm.* **72**: 370–377.

Kroll A, Pillukat MH, Hahn D, Schnekenburger J. 2012. Interference of engineered nanoparticles with in vitro toxicity assays. *Arch. Toxicol.* **86**: 1123–1136.

Kumar V, Gill KD. 2009. Aluminium neurotoxicity: neurobehavioural and oxidative aspects. *Arch. Toxicol.* **83**: 965–978.

Lanone S, Rogerieux F, Geys J, Dupont A, Maillot-Marechal E, Boczkowski J, Lacroix G, Hoet P. 2009. Comparative toxicity of 24 manufactured nanoparticles in human alveolar epithelial and macrophage cell lines. *Part. Fibre Toxicol.* **6**: 14.

Luengo Y, Nardecchia S, Morales MP, Serrano MC. 2013. Different cell responses induced by exposure to maghemite nanoparticles. *Nanoscale* **5**: 11428–11437.

Monteiro-Riviere NA, Inman AO, Zhang LW. 2009. Limitations and relative utility of screening assays to assess engineered nanoparticle toxicity in a human cell line. *Toxicol. Appl. Pharmacol.* **234**: 222–235.

Morsy GM, Abou El-Ala KS, Ali AA. 2013. Studies on fate and toxicity of nanoalumina in male albino rats: oxidative stress in the brain, liver and kidney. *Toxicol. Ind. Health* Epub ahead of print.

Nel A, Xia T, Mädler L, Li N. 2006. Toxic potential of materials at the nanolevel. *Science* **311**: 622–627.

Nel AE, Mädler L, Velegol D, Xia T, Hoek EM, Somasundaran P, Klaessig F, Castranova V, Thompson M. 2009. Understanding biophysicochemical interactions at the nano-bio interface. *Nat. Mater.* **8**: 543–557.

Nel A, Xia T, Meng H, Wang X, Lin S, Ji Z, Zhang H. 2013. Nanomaterial toxicity testing in the 21st century: use of a predictive toxicological approach and high-throughput screening. *Acc. Chem. Res.* **46**: 607–621.

Oberdörster G, Oberdörster E, Oberdörster J. 2005. Nanotoxicology: an emerging discipline evolving from studies of ultrafine particles. *Environ. Health Perspect.* **113**: 823–839.

Pailleux M, Boudard D, Pourchez J, Forest V, Grosseau P, Cottier M. 2013. New insight into artifactual phenomena during in vitro toxicity assessment of engineered nanoparticles: study of TNF-a adsorption on alumina oxide nanoparticle. *Toxicol. In Vitro* **27**: 1049–1056.

Panariti A, Miserocchi G, Rivolta I. 2012. The effect of nanoparticle uptake on cellular behavior: disrupting or enabling functions? *Nanotechnol. Sci. Appl.* **5**: 87–100.

Park EJ, Kim H, Kim Y, Choi K. 2010. Repeated-dose toxicity attributed to aluminum nanoparticles following 28-day oral administration, particularly on gene expression in mouse brain. *Toxicol. Environ. Chem.* **93**: 120–133.

Park EJ, Shim JH, Kim Y, Han BS, Yoon C, Lee S, Cho MH, Lee BS, Kim JH. 2015. A 13-weeks repeated dose oral toxicity and bioaccumulation of aluminum oxide nanoparticles in mice. *Arch. Toxicol.* **89**: 371–379.

Park EJ, Umh HN, Choi DH, Cho MH, Choi W, Kim SW, Kim Y, Kim JH. 2014b. Magnetite- and maghemite-induced different toxicity in murine alveolar macrophage cells. *Arch. Toxicol.* **88**: 1607–1618.

Park EJ, Lee GH, Shim JH, Cho MH, Lee BS, Kim YB, Kim JH, Kim Y, Kim DW. 2014. Comparison of the toxicity of aluminum oxide nanorods with different aspect ratio. *Arch. Toxicol.* Epub ahead of print.

Radzium E, Dudkiewicz Wilczyńska J, Książek I, Nowak K, Anuszewska EL, Kunicki A, Olszyna A, Ząbkowski T. 2011. Assessment of the cytotoxicity of aluminum oxide nanoparticles on selected mammalian cells. *Toxicol. In Vitro* **25**: 1694–1700.

Roh HS, Choi GK, An JS, Cho CM, Kim DH, Park IJ, Noh TH, Kim DW, Hong KS. 2011. Size-controlled synthesis of monodispersed mesoporous α-alumina spheres by a template-free forced hydrolysis method. *Dalton Trans.* **40**: 6901–6905.

Sun J, Wang S, Zhao D, Hun FH, Weng L, Liu H. 2011. Cytotoxicity, permeability, and inflammation of metal oxide nanoparticles in human cardiac microvascular endothelial cells: cytotoxicity, permeability, and inflammation of metal oxide nanoparticles. *Cell Biol. Toxicol.* **27**: 333–342.

Wagner AJ, Bleckmann CA, Murdock RC, Schrand AM, Schlager JJ, Hussain SM. 2007. Cellular interaction of different forms of aluminum nanoparticles in rat alveolar macrophages. *J. Phys. Chem. B* **111**: 7353–7359.

Walkey CD, Chan WC. 2012. Understanding and controlling the interaction of nanomaterials with proteins in a physiological environment. *Chem. Soc. Rev.* **41**: 2780–2799.

Yue MB, Xue T, Jiao WQ, Wang YM, He MY. 2011. CTAB-directed synthesis of mesoporous g-alumina promoted by hydroxyl carboxylate: The interplay of tartrate and CTAB. *Solid State Sci.* **13**: 409e416.

Zhang QL, Li MQ, Ji JW, Gao FP, Bai R, Chen CY, Wang ZW, Zhang C, Niu Q. 2011. In vivo toxicity of nano-alumina on mice neurobehavioral profiles and the potential mechanisms. *Int. J. Immunopathol. Pharmacol.* **24**(1 Suppl): 23S–29S.

Supporting information

Additional supporting informationmay be found in the online version of this article at the publisher's website.